أكاديمية كاوست
KAUST ACADEMY

جامعة الملك عبدالله
للعلوم والتقنية
King Abdullah University of
Science and Technology

Design and Thermodynamic Evaluation of a Cascaded Waste Heat Recovery System with Thermal Energy Storage

Hatim AlRafei, Prof. Andy Woods

hatim.alrafei@kaust.edu.sa, aww1@cam.ac.uk

Abstract

Industrial processes produce waste heat at different temperature levels; therefore, there is an option to enhance energy efficiency via waste heat recovery and thermal energy storage (TES). In this work, a cascade system of industrial waste heat recovery combined with TES is studied, where the heat obtained can be utilized based on the process requirements depending on the temperature level. Three potential storage media are selected: basalt rocks for sensible heat storage, Solar Salt for latent heat storage, and magnesium sulfate hydrate for thermochemical storage. Transient simulations are carried out for a 1 MWh basalt sensible heat storage unit using basalt rods with a diameter of 30 mm and a length of 3 m, with air acting as a heat carrier.

The process of charging and discharging was modeled for an eight-hour time span, including discharge by reverse flow and cycling of charge and discharge operations. Following the initial charging, the mean temperature of the basalt reached 496.78°C, and approximately 0.7936 MWh of heat was accumulated, which corresponds to 79.36% of the theoretical 1 MWh of heat accumulation. In the first reverse flow discharge, approximately 0.6538 MWh of heat was recovered, and the recovery ratio is 82.39%.

From the ten cycles of simulation, the cyclic steady state was achieved around the fourth or fifth cycle. At steady state, the mean net heat added during charging and the heat recovered during the discharging cycles stabilized at around 0.6897 MWh per cycle. Because there are no external heat losses or thermal radiation in the numerical model, the cycle recovery efficiency reaches 100%.

Date: August 20, 2026

Contents

1 Introduction **2**

1.1 Industrial Decarbonization & Waste Heat Classification . . . 2

1.2 Thermal Energy Storage (TES) Principles . . . 2

1.3 Cascaded Thermal Energy Storage (TES) Concept . . . 3

2 Related Work **3**

2.1 Technical & Thermodynamic Criteria . . . 3

2.2 Candidate Material Pathways . . . 4

2.3 Comparative Analysis of Candidate Materials . . . 4

2.4 Selection Rationale for Specific Material Compositions . . . 5

3 Methodology **5**

3.1 System Integration and Inline Thermal Buffering . . . 5

3.2 Basalt Thermal Energy Storage Tank Design . . . 6

3.3 Governing Equations and Transient Thermal Model . . . 7

4 Results **9**

4.1 Baseline Design Results . . . 9

4.2 Airflow and Convective Heat Transfer Results . . . 11

4.3 Charging Temperature Results . . . 12

4.4 Discharging Results . . . 14

4.5 Repeated Charge–Discharge Cycle Analysis . . . 15

4.6 Thermal Energy Recovery . . . 17

5 Discussion **17**

6 Limitations and Future Work **19**

7 Conclusion **19**

References **20**

1 Introduction

1.1 Industrial Decarbonization & Waste Heat Classification

The global industrial processes utilize a large share of the world's primary energy, which also produces considerable quantities of industrial waste heat streams in the form of high temperatures. The lack of exhaust stream recovery is one of the main energetic and exergetic losses that exacerbate green-house gas emissions and industrial inefficiency. Therefore, decarbonization of industrial manufacturing calls for rigorous Waste Heat Recovery (WHR) measures capable of recycling the thermal cascades and integrating them back into production flows.

Waste heat streams may be defined according to their thermodynamic temperature regimes: High Temperature Exhausts (> 500°C), Medium Temperature Streams (200°C–500°C), and Low Temperature Effluents (< 200°C). Although high temperature heat streams possess a better thermodynamic quality (exergy), low and medium-grade waste heat streams are predominant at the majority of facilities. Efficient WHR process design should consider these thermodynamic regimes.

Table 1 Classification of Industrial Waste Heat by Temperature Regimes

Temperature Category	Operational Window	Typical Industrial Sources
High-Grade Heat	> 500°C	Glass melting furnaces, cement kilns, steel re-heating processes
Medium-Grade Heat	200°C–500°C	Gas turbine exhaust, steam boiler flue gas, catalytic crackers
Low-Grade Heat	< 200°C	Cooling jacket water, condensing flue gas, process effluents

1.2 Thermal Energy Storage (TES) Principles

The importance of Thermal Energy Storage (TES) in contemporary energy systems is hardly disputable since TES serves as an effective thermal energy storage technology that helps to connect the gap between heat generation and consumption processes. If the energy recovery process is involved in the industrial facility operation, the availability and temperature of the recovered thermal energy rarely match the requirements of the downstream process. As a result, TES systems allow storing the excess energy when the need for it is not so high and utilizing it when it is required.

At a fundamental thermodynamic level, TES systems operate through three main mechanisms, categorized by their storage medium and operational physics:

- **Sensible Heat Thermal Energy Storage (SHTES):** Thermal energy is stored by heating the medium without changing its phase, which is controlled by $Q = mC_p\Delta T$. It operates over a wide range of temperatures (100°C to > 800°C) and can use simple and inexpensive materials such as rocks, concrete, ceramics, molten salts, and heat transfer oils but requires large volume sizes and delivers varying temperatures from the storage.
- **Latent Heat Thermal Energy Storage (LHTES):** Uses the latent heat gained or lost during phase change processes at near-constant temperatures. The operating temperature depends on the selected Phase Change Material (PCM), whose phase-change temperature is chosen according to the intended application. Phase Change Materials (PCMs) like paraffin waxes

and eutectic metals provide increased energy density and isothermal release, even though they have low thermal conductivity.

- **TCES (Thermochemical Energy Storage):** Energy stored via reversible chemical reactions or by sorption phenomena (such as $MgSO_4 \cdot nH_2O$). Depending on the selected reaction system, TCES can operate over a wide temperature range; however, $MgSO_4 \cdot 7H_2O$, selected in this study, is intended for low-temperature applications below approximately 200°C. TCES offers very high energy densities and is loss-free and long-term energy storage, although there are challenges related to kinetics and complexities of the process.

1.3 Cascaded Thermal Energy Storage (TES) Concept

Single-stage heat recovery systems may lack thermodynamic efficiency in the utilization of high-temperature waste streams to produce low-quality process heat. If there is a big ΔT difference between the source of thermal energy and its application point, much exergy will be destroyed in the process.

To improve thermodynamic efficiency, the Cascaded Thermal Energy Storage (CTES) approach utilizes thermal energy at different temperature levels according to process heat requirements, as follows:

- **Exergy-Matched Storage:** The storage device stores the waste heat collected by the system and maintains its thermal exergy content, thereby enabling energy utilization based on temperature quality and not immediate availability.
- **Cascaded Distribution Network:** Heat extracted from the storage bed is dispatched sequentially across process utility tiers:
  1. **High-Grade Tier:** High-grade thermal energy is supplied to high-temperature process heating or high-pressure steam generation.
  2. **Medium-Grade Tier:** Medium-temperature heat is cascaded through the process utility network.
  3. **Low-Grade Tier:** The low-grade heat is used for pre-heating of the feedstock stream.

The above method of energy distribution based on thermal supply matching enables minimization of temperature differential (ΔT) and reduction in exergy loss, thereby improving overall thermal utilization and reducing exergy destruction within the facility.

2 Related Work

2.1 Technical & Thermodynamic Criteria

Choosing the best medium to recover thermal energy with efficiency depends on assessing many different thermodynamic, physical, and economic factors. In order to operate safely, reliably, and economically within an industrial process, each candidate material is evaluated against five primary selection criteria [6]:

- **Specific Heat Capacity, Latent Heat, or Reaction Enthalpy:** The relevant energy storage parameter depends on the storage mechanism employed. Sensible storage materials are evaluated using specific heat capacity, latent storage materials using latent heat of fusion, and thermochemical materials using reaction enthalpy.
- **Volumetric Energy Density:** It represents the amount of energy storage per unit volume of the material. Volumetric energy density should be high in order to decrease the size of the vessel as well as reduce the cost involved in its construction.

- **Thermal Conductivity (k):** It represents the rate of heat absorption and release. A high thermal conductivity allows faster heat transfer by reducing thermal resistance, resulting in shorter charging and discharging times without requiring additional heat transfer surfaces.
- **Thermal Stability and Operating Window:** It represents the upper limit up to which the material can tolerate thermal decomposition or phase separation. Its operating temperature range should be compatible with the temperature of the intended waste heat source.
- **Cost, Availability, and TRL:** This criterion considers the economic feasibility, material availability, and technology readiness level (TRL) of each candidate material.

2.2 Candidate Material Pathways

Three candidate materials for thermal energy storage were selected for evaluation within the proposed CTES system. Each material is unique in that it uses a specific thermal energy storage mechanism (sensible, latent, or thermochemical), and all three are evaluated as an alternative storage material for the TES tank.

For high-temperature TES applications, the sensible heat storage material is Basalt Rocks. Basalt Rocks are evaluated as the sensible heat storage candidate because of their excellent thermal stability (> 800°C), good thermal conductivity (1.5–2.5 W/m·K), mechanical strength, and low material cost [1].

For medium-temperature TES applications, the selection of latent heat storage material is Nitrate Molten Salts (Solar Salt: 60% $NaNO_3$/40% KNO_3). Solar Salt has been chosen because of its melting point of 220°C and its latent heat of fusion of 160 kJ/kg [2].

For low-temperature TES applications, Magnesium Sulfate Hydrates ($MgSO_4{\cdot}7H_2O$) are being considered for their use in low temperature applications in the TES system. The system works by undergoing a reversible hydration/dehydration process at temperatures lower than 200°C and boasts extremely high energy density approximately 1000 MJ/m^3 [3].

Although each material is particularly suitable for a specific temperature range, all three materials are evaluated as alternative storage media for the same TES tank.

2.3 Comparative Analysis of Candidate Materials

To evaluate the suitability of each selected medium within the proposed Thermal Energy Storage (TES) system, Table 2 presents a side-by-side comparison across key thermodynamic, operating, and technological parameters [1–3].

Table 2 Comparative analysis of the candidate TES materials

Parameter/Feature	High-Temperature (Basalt)	Medium-Temperature (Solar Salt)	Low-Temperature ($MgSO_4 \cdot 7H_2O$)
Candidate Material	Basalt Rocks	Nitrate Molten Salt (60% $NaNO_3$/40% KNO_3)	Magnesium Sulfate Hydrates ($MgSO_4 \cdot 7H_2O$)
Storage Mechanism	Sensible Heat	Latent Heat	Thermochemical Heat
Operating Temperature Range	Thermally stable above 800°C	Melting point ≈ 220°C	< 200°C
Thermal Conductivity	1.5–2.5 W/m·K	≈ 0.5 W/m·K	Low (Matrix-dependent)

Parameter/Feature	High-Temperature (Basalt)	Medium-Temperature (Solar Salt)	Low-Temperature ($MgSO_4 \cdot 7H_2O$)
Energy Density	Moderate	High (Latent Heat $\approx$ 160 kJ/kg)	Very High (> 1000 MJ/m^3)
Typical Application	High-temperature sensible heat storage	Medium-temperature latent heat storage	Long-term thermochemical heat storage
Technology Readiness Level (TRL)	TRL 8–9	TRL 8–9	TRL 3–5
Cost & Availability	Very low cost / Abundant	Moderate cost / Commercially available	Low raw material cost / Complex system integration

2.4 Selection Rationale for Specific Material Compositions

2.4.1 Why Solar Salt (60% $NaNO_3$/40% KNO_3)?

Solar Salt is an optimal choice for commercial applications among molten salt blends. Although chloride salts have the capacity to reach higher operating temperatures, they are highly corrosive and require expensive nickel-based alloys. Carbonate salts, on the other hand, carry significantly higher material costs. The key advantages of Solar Salt include its low melting point ($\approx$ 220°C), non-corrosive behavior with standard stainless steel, and high thermal stability up to 565°C [2].

2.4.2 Why Basalt Rocks?

Basalt rocks have greater resistance to thermal shock than other materials such as concrete, granite and cast iron since they exhibit good resistance to thermal shock during repeated heating and cooling cycles. In addition, basalt has higher mechanical compressive strength, chemical inertness in high-temperature gases flow, and very low cost of raw material since it is naturally available [1,4].

2.4.3 Why Magnesium Sulfate Hydrate ($MgSO_4 \cdot 7H_2O$)?

Among the candidate materials considered for low-temperature TES applications, such as $CaCl_2$ and $MgCl_2$, ($MgSO_4 \cdot 7H_2O$) was chosen due to its safe, non-corrosive, and environmentally friendly nature, along with a high energy density of approximately 1 GJ/m^3. More importantly, the reaction kinetics of this salt are activated at relatively low dehydration temperatures (100–150°C), reducing the deliquescence and slurrying issues commonly associated with chloride salts [3].

3 Methodology

3.1 System Integration and Inline Thermal Buffering

High-temperature industrial energy systems that employ waste heat recovery (WHR) or high-temperature process streams experience severe transient dynamics. Process fluctuation, intermittent flue-gas emissions, and cycling schedules contribute to large discrepancies between the thermal energy supply and process needs. Directly linking such transients can cause destabilization of high-temperature industrial process equipment, initiate thermal stress leading to mechanical fatigue, and reduce the overall efficiency of the system.

To manage the operational dynamics described, the integrated design incorporates an inline thermal buffering concept. The direct coupling of the raw thermal streams to the end-user process

equipment is avoided through the incorporation of a TES system as an intermediate thermal battery.

The inline thermal battery serves two fundamental roles:

- **Transient Stabilization:** It handles sudden temperature peaks and large mass flows from the energy source, thereby ensuring smooth thermal energy supply profiles before supplying a more stable heat supply to the downstream process.
- **Decoupling Energy Supply and Demand:** It facilitates temporal decoupling, which means that the energy collection system operates independently of the immediate demand at the plant.

3.2 Basalt Thermal Energy Storage Tank Design

3.2.1 Design Basis and Modelling Assumptions

The objective is to create an initial thermal design for the proposed sensible heat storage tank based on basalt as a heat storage material. The engineering calculations help estimate the parameters of the heat storage tank and its transient thermal behavior during charge-discharge process.

The selected storage material is basalt, which has the ability to store energy in the form of sensible heat and does not experience any phase change. Thus, the amount of energy stored will depend on the mass of basalt, specific heat capacity, and temperature difference [1].

In the storage medium, parallel cylinders of basalt rods have been used inside the insulated cylindrical storage tank. Hot air has been chosen as the heat transfer fluid (HTF). The airflow rate is determined using a literature-based scaling approach rather than being selected arbitrarily, and it moves axially through the passages of the rods. In charging mode, the thermal energy is supplied to the basalt rods from hot air. During discharging, both same-flow and reverse-flow configurations were evaluated, with reverse-flow subsequently selected based on the predicted thermal recovery performance.

Unlike lumped systems in which the temperature is assumed to be uniform across the whole storage medium, the current study takes into consideration the temperature variation along the storage tank. For this reason, the storage tank is divided into several axial control volumes where the transient temperature distribution is calculated based on time and axial location.

3.2.2 Storage Tank Configuration

The energy storage tank is made up of an insulated cylindrical container that has basalt rods placed parallelly within it. These rods have been placed in the direction of air flow so as to provide straight pathways for heat transfer fluid through the tank. This arrangement makes it easier for the temperature distribution along the tank length to be analyzed numerically [5].

During the charging process, air at about 600°C flows into the inlet manifold and loses thermal energy by means of forced convection through heating the basalt rods around it. When the air moves through the storage vessel, its temperature gradually decreases since a portion of its thermal energy is continually being transferred to the storage media. This is why the initial rod segments are heated faster than the subsequent ones.

In the process of discharging, the direction of flow of air changes. Cold air enters into the storage chamber, picks up heat energy from the heated basalt rods and leaves the chamber at a high temperature.

To account for such non-uniform thermal behavior, the storage tank is subdivided into many axial control volumes, each of which interacts independently with the ambient airflow in order to calculate the temperature evolution of both the airflow and the basalt.

3.3 Governing Equations and Transient Thermal Model

The storage unit was divided into several segments in the axial direction; thus the temperatures of the air and basalt could change in the axial direction and also with time.

Unlike the steady-state model, the transient equation considers the progressive advancement of the thermal front during charge and discharge operations. At the onset of the charging operation, the whole basalt formation is considered to have the initial temperature. With the passage of hot air inside the storage chamber, the transfer of heat takes place from hot air to each basalt element such that the air temperature drops but the basalt temperature rises gradually.

The governing equations are based on the conservation of energy for both the storage medium and the heat transfer fluid.

3.3.1 Sensible Heat Storage Equation

Since basalt stores thermal energy by sensible heat only, the theoretical storage capacity is calculated from [6].

$$E = m_s C_{p,s} \Delta T \tag{1}$$

where:

- E is stored thermal energy (J),
- m_s is the basalt mass (kg),
- $C_{p,s}$ is the specific heat capacity of basalt (J/kg·K),
- ΔT is the operating temperature difference (K).

For the present study,

$$\Delta T = T_{hot} - T_{cold} \tag{2}$$

where

$$T_{hot} = 600^{\circ}C$$

and

$$T_{cold} = 100^{\circ}C.$$

This equation was used to determine the required basalt mass for the selected storage capacity before constructing the numerical model.

3.3.2 Basalt Energy Balance

Each basalt rod was divided into a number of axial control volumes. The transient temperature variation of each control volume is governed by the following energy balance:

$$\rho_s C_{p,s} V_s \frac{\partial T_s}{\partial t} = hA(T_a - T_s) \tag{3}$$

where:

- ρ_s is the basalt density,
- $C_{p,s}$ is the basalt specific heat,
- V_s is the volume of the control volume,
- h is the convective heat transfer coefficient,

- A is the heat transfer surface area,
- T_a is the local air temperature,
- T_s is the local basalt temperature.

The left-hand side represents the rate of thermal energy stored inside the basalt segment, whereas the right-hand side represents the convective heat transferred from the hot air to the basalt surface.

As charging progresses, the basalt temperature increases as heat is transferred from the flowing air. Due to the finite charging duration and the axial temperature variation, complete thermal equilibrium is not necessarily reached.

3.3.3 Air Energy Balance

The heat lost by the airflow is equal to the heat gained by the basalt segment. Therefore, the local air energy balance is expressed as

$$\dot{m}_a C_{p,a}(T_{a,in} - T_{a,out}) = hA(T_a - T_s) \tag{4}$$

where:

- $\dot{m}_a$ is the air mass flow rate,
- $C_{p,a}$ is the air specific heat,
- $T_{a,in}$ is the inlet air temperature of the segment,
- $T_{a,out}$ is the outlet air temperature of the segment.

This equation describes the reduction in air temperature as thermal energy is transferred to the basalt rods.

During charging,

$$T_{a,out} < T_{a,in} \tag{5}$$

because the airflow continuously loses thermal energy while travelling through the storage tank.

3.3.4 Axial Temperature Distribution

Since the airflow continuously transfers heat to the storage medium, the temperatures of both the air and the basalt vary along the storage tank length.

Therefore,

$$T_a = T_a(z, t) \tag{6}$$

and

$$T_s = T_s(z, t) \tag{7}$$

where z is the axial position measured along the rod length and t is time.

This formulation produces a moving thermal front inside the storage tank. The basalt located near the inlet is heated first, whereas the downstream sections experience a delayed temperature rise.

For the discharging process, the flow of thermal front is governed by the flow chosen for the process. This research considers both same flow and opposite flow directions to identify the more efficient thermal energy recovery.

3.3.5 Numerical Discretization

To solve the transient equations, the storage tank was divided into a finite number of axial segments. The 3 m storage length was divided into 20 equal axial segments, giving a segment length of 0.15 m. Each segment exchanges heat independently with the surrounding airflow.

The transient solution proceeds sequentially in time. At every time step:

1. The inlet air temperature of each segment is known.
2. The heat transferred from the air to the basalt is calculated using the local temperature difference.
3. The basalt temperature is updated.
4. The outlet air temperature becomes the inlet temperature for the following segment.

This procedure is repeated until the desired charging or discharging time is reached.

The temperature of the basalt at the next time step is evaluated using the explicit time-marching equation

$$T_s^{n+1} = T_s^n + \frac{\dot{Q}_{seg}\Delta t}{m_{seg}C_{p,s}} \tag{8}$$

where:

- $\dot{Q}_{seg}$ is the heat transferred during one time step,
- Δt is the numerical time step,
- m_{seg} is the mass of one basalt segment.

Similarly, the air temperature leaving each segment is calculated sequentially and used as the inlet temperature of the next segment.

4 Results

4.1 Baseline Design Results

The preliminary calculations of design were made according to the assumptions of the design stated previously. The aim of these calculations is to estimate the quantity of basalt needed for obtaining the desired capacity and to define the basic parameters of the tank's geometry. The below-mentioned calculations give the theoretical values of the initial design, considering the assumptions of basalt homogeneity and sensible heat storage.

4.1.1 Required Basalt Mass

The required basalt mass was determined using the sensible heat storage equation

$$E = m_s C_{p,s}\Delta T \tag{9}$$

where the design storage capacity was selected as 1 MWh, the basalt specific heat capacity was assumed to be 850 J/kg·K [1], and the operating temperature difference was 500 K (600°C–100°C).

Rearranging the equation,

$$m_s = \frac{E}{C_{p,s}\Delta T} \tag{10}$$

Substituting the selected design values gives

$$m_s = \frac{3.6 \times 10^9}{850 \times 500} = 8470.59 \text{ kg} \tag{11}$$

The computed value of basalt weight corresponds to the theoretical weight required for uniform heating of the storage system from 100°C to 600°C. However, the temperature distribution within the storage container is not uniform when charging takes place; hence, the actual energy stored is dependent on the transient temperature distribution.

4.1.2 Basalt Rod Geometry

For the selected baseline design,

- Rod diameter = 30 mm
- Rod length = 3 m

The volume of one basalt rod is calculated from

$$V_{rod} = \frac{\pi D^2}{4} L \tag{12}$$

Substituting the selected dimensions,

$$V_{rod} = 0.002121 \text{ m}^3 \tag{13}$$

The corresponding rod mass is

$$m_{rod} = \rho_s V_{rod} \tag{14}$$

which gives

$$m_{rod} = 5.94 \text{ kg} \tag{15}$$

4.1.3 Required Number of Basalt Rods

The total number of rods required was estimated by dividing the total basalt mass by the mass of one rod:

$$N = \frac{m_{total}}{m_{rod}} \tag{16}$$

$$N = \frac{8470.59}{5.94} = 1426.60 \tag{17}$$

Since only whole rods can be used,

$$N = 1427 \text{ rods} \tag{18}$$

The relatively high number of rods provides for a higher heat transfer area and uniform exchange of heat with the moving air.

4.1.4 Estimated Storage Volume

The total solid volume occupied by the basalt is determined from

$$V_s = \frac{m_s}{\rho_s} \tag{19}$$

Substituting the calculated values,

$$V_s = \frac{8470.59}{2800} = 3.025\ \text{m}^3 \tag{20}$$

Thus, the basalt occupies approximately 3.03 m^3. This is just the calculated volume for the basalt solids. In reality, there will be an extra volume needed for the passages for air flow, the inlet and outlets, the manifolds and the insulation within the tank.

4.2 Airflow and Convective Heat Transfer Results

The airflow required for the present storage system was scaled according to the ratio of storage masses and charging durations. The calculated air mass flow rate was

$$\dot{m}_a = 0.251497\ \text{kg/s} \tag{21}$$

A pitch-to-diameter ratio of 1.5 was selected for the rod arrangement [5]:

$$\frac{P}{D} = 1.5 \tag{22}$$

Since the rod diameter is 0.030 m,

$$P = 1.5(0.030) = 0.045\ \text{m} \tag{23}$$

Therefore, the clear gap between adjacent rods is

$$Gap = 0.045 - 0.030 = 0.015\ \text{m} \tag{24}$$

The calculated total free-flow area was

$$A_{free,total} = 1.88099\ \text{m}^2 \tag{25}$$

and the corresponding average air velocity was

$$U = 0.273985\ \text{m/s} \tag{26}$$

The calculated hydraulic diameter was

$$D_h = 0.055944\ \text{m} \tag{27}$$

The Reynolds number was calculated as

$$Re = 219.73 \tag{28}$$

while the Prandtl and Graetz numbers were

$$Pr = 0.707 \tag{29}$$

$$Gz = 2.90 \tag{30}$$

Using the Hausen correlation for thermally developing laminar flow [7], the Nusselt number was calculated as

$$Nu = 3.839 \tag{31}$$

Finally, the convective heat transfer coefficient between the air and basalt rods was

$$h = 3.568\ \mathrm{W/m^2K} \tag{32}$$

4.3 Charging Temperature Results

The transient charging process was simulated for eight hours. All basalt segments were initially at 100°C, while hot air was continuously supplied at 600°C.

According to the numerical results, a non-uniform temperature distribution was obtained in the storage tank. The segments of basalt in close proximity to the inlet experienced higher heating due to their continuous contact with high-temperature air. Segments far from the inlet received lower-temperature air; therefore, their heating was slower.

4.3.1 Basalt Temperature Profile

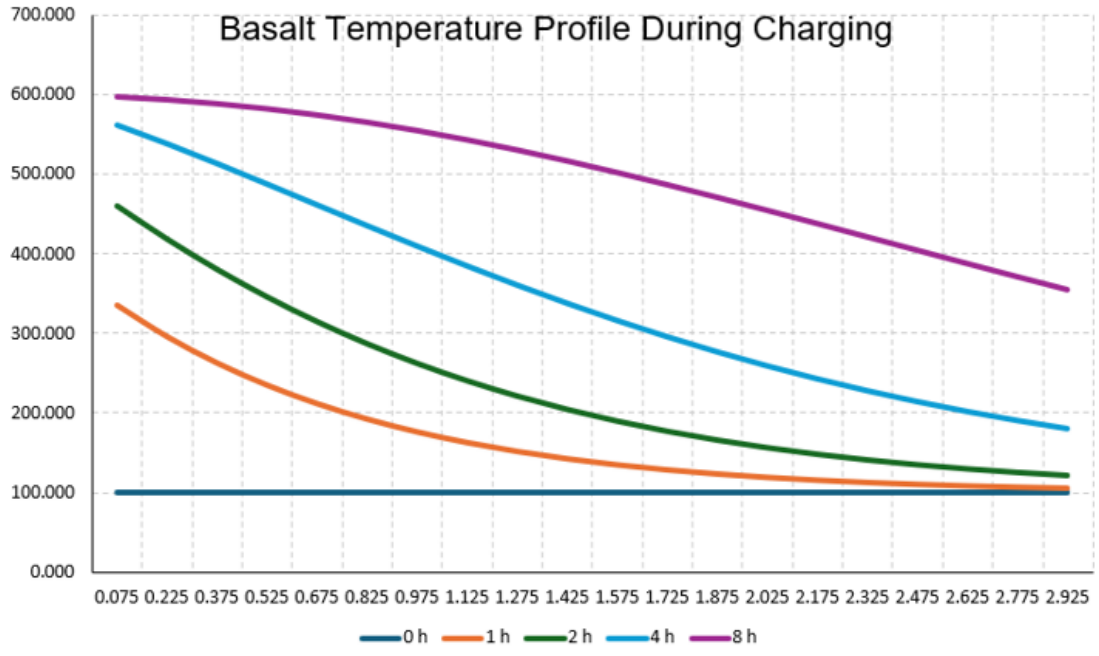


Figure 1 Basalt temperature profiles along the storage tank during charging.

Figure 1 presents the basalt temperature distribution along the storage tank at charging times of 0, 1, 2, 4, and 8 hours.

At the start of the charging process, the entire basalt medium was at a temperature of 100°C. However, after an hour had elapsed, the temperature had risen significantly in only the segments close to the air inlet region.

As the charging process proceeded, the region of high temperature kept extending itself gradually down the length of the tank. The graphs of temperature at two, four, and eight hours show the motion of the heat wave towards the outlet.

The calculated average basalt temperature at the end of the eight-hour charging period was

$$T_{s,avg} = 496.779°C \tag{33}$$

The energy storage medium did not achieve the same temperature of 600°C. This indicates that the theoretical capacity determined by the increase in temperature is the maximum capacity achievable, not the actual amount of energy stored within a certain period of time.

4.3.2 Air Temperature Profile

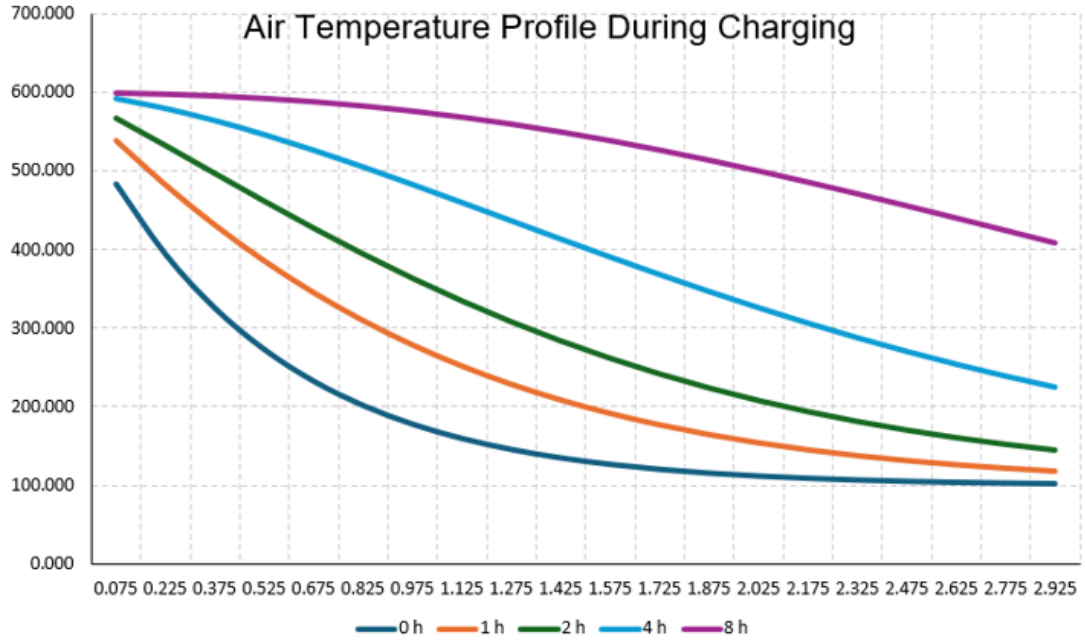


Figure 2 Air temperature profiles along the storage tank during charging.

The air temperature at the tank inlet was kept at 600°C during the entire charging process. After that, the air temperature gradually decreased along the flow direction as heat was transferred from the air to the basalt segments.

During the initial stages of charging, the basalt was cold and hence, able to absorb most of the heat energy provided by the air. Therefore, the outlet air temperature was almost the same as that of the basalt temperature at the beginning. With the rise in temperature of the basalt rods, the difference in temperature of the air and basalt reduced, causing an increase in outlet air temperature.

At the end of the eight-hour charging period, the outlet-air temperature was

$$T_{a,out} = 407.67°C \tag{34}$$

The relatively high temperature at the outlet suggests that some of the supplied heat energy stayed in the air flow without being absorbed by the basalt over the charging period.

4.3.3 Charging Temperature History

The mean temperatures of basalt and the outlet air both rose continually for the entire eight-hour charging process. The temperature of the basalt increased since there was transfer of heat energy from the hot air to the storage media. This happened as the temperature difference between the air and basalt kept reducing during the process of charging.

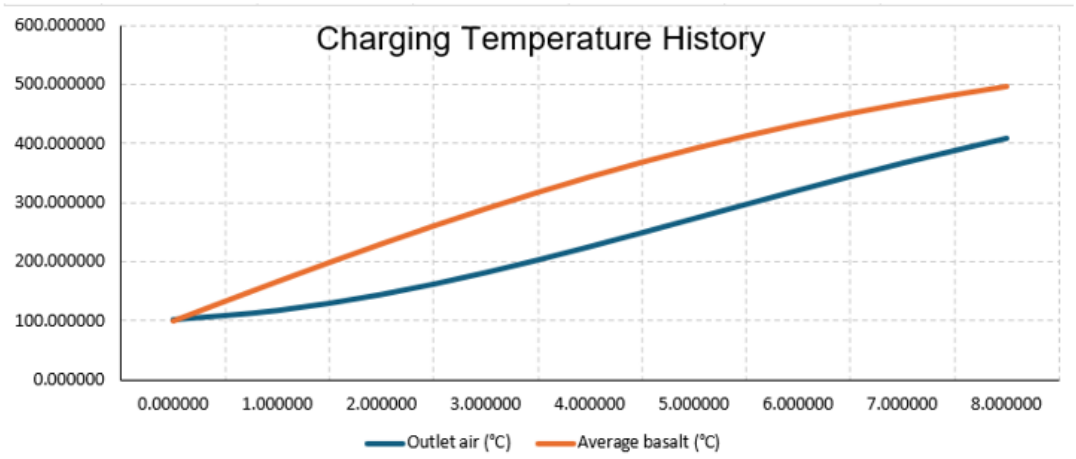


Figure 3 Average basalt and outlet-air temperature history during the eight-hour charging period.

Towards the end of the charging period, the average basalt temperature reached approximately 496.78°C, while the outlet-air temperature reached approximately 407.67°C.

4.4 Discharging Results

After the charging operation, the thermal energy accumulated inside the basalt rods was extracted by means of a reverse flow discharge process. Cooler air at an inlet temperature of 100°C was fed to the storage tank from the other end.

Two different discharges were analyzed, one where the discharge is in the same direction of the flow of air during charging and another where the discharge is in the opposite direction of the flow of air during charging. These two discharges were modeled with the same inlet air condition, flow rate, heat transfer coefficient, and discharge time.

Based on the comparison, reverse-flow discharge provided better thermal recovery performance and was therefore selected for the subsequent discharge and repeated-cycle analyses.

4.4.1 Reverse-Flow Discharging Temperature History

In the early discharge process, the outlet-air temperature was quite high since the cool air came into contact with the hot basalt rods in the reverse flow direction at the inlet side. With the dissipation of thermal energy in the storage medium, both the basalt and outlet-air temperatures reduced gradually.

The average temperature of the basalt dropped from around 496.78°C at the start of discharging to around 169.87°C after eight hours. The outlet-air temperature decreased throughout the discharge period, reaching approximately 237.23°C after eight hours.

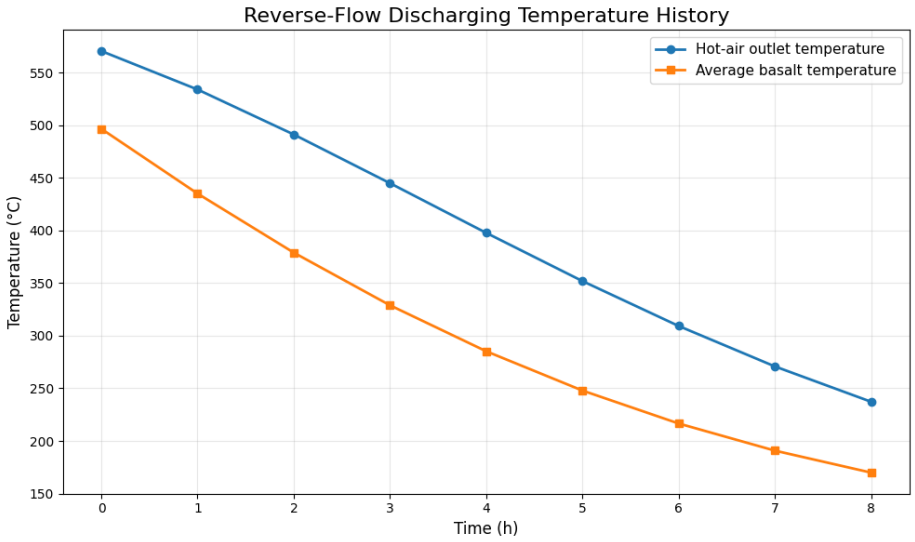


Figure 4 Reverse-flow discharging temperature history showing the hot-air outlet temperature and average basalt temperature over the eight-hour discharge period.

4.5 Repeated Charge–Discharge Cycle Analysis

The evaluation of the long-term thermal performance of the storage system involved extending the transient model to ten cycles of charge-discharge. Each cycle involved an 8-hour period of charging followed by an 8-hour period of reverse flow discharging. The final temperature distribution of the basalt at the end of each discharge was used as the initial condition of the charging process in the next cycle. In other words, the storage medium did not return to its original temperature of 100°C between each cycle.

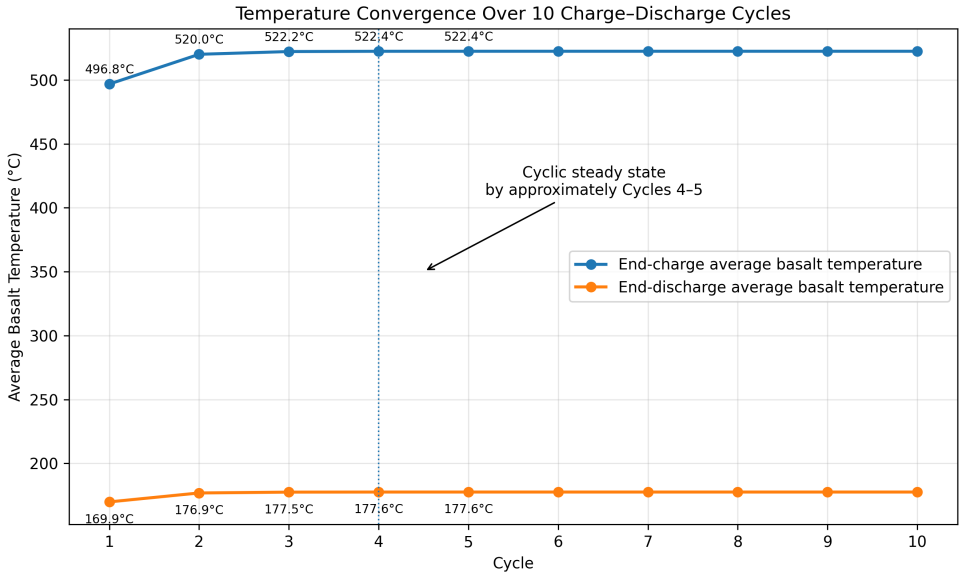


Figure 5 End-of-charge and end-of-discharge average basalt temperatures over ten charge–discharge cycles, showing convergence toward cyclic steady-state operation.

During the first cycle, the average basalt temperature rose from 100°C to approximately 496.78°C due to charging, but it then dropped to approximately 169.87°C due to reverse flow

discharging for eight hours. Because the basalt held heat even after the discharge, the starting point of the second cycle was from a high temperature level than the starting temperature of 100°C.

The average basalt temperatures at end of charge and discharge during subsequent cycles reached stable values as the number of cycles increased. By approximately Cycles 4–5, there was no appreciable change in the temperature from one cycle to another. In cyclic steady state, the end-of-charge average basalt temperature reached approximately 522.42°C, while the end-of-discharge average basalt temperature reached approximately 177.58°

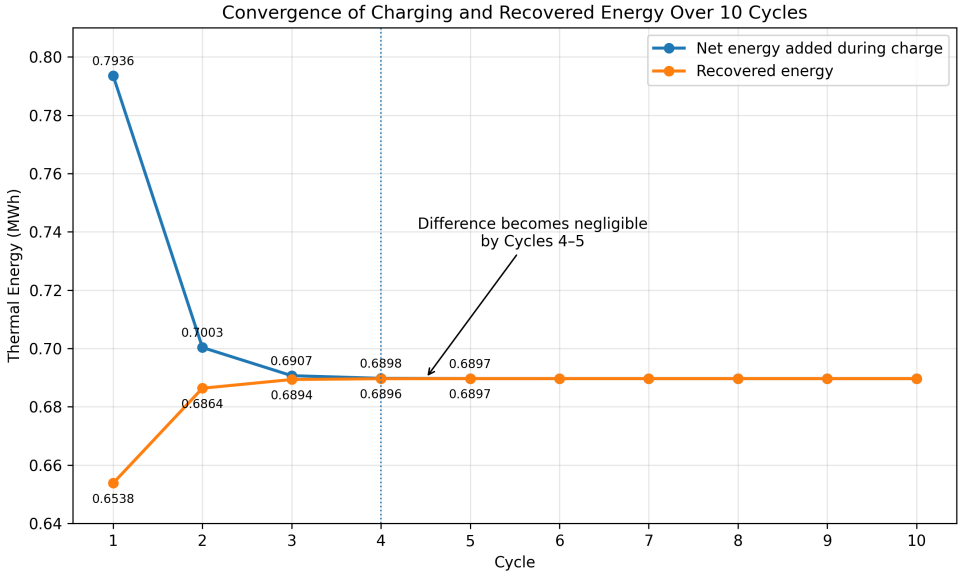


Figure 6 Convergence of the net thermal energy added during charging and the recovered thermal energy over ten charge–discharge cycles.

The energy results demonstrated similar convergent behavior. For Cycle 1, there was an addition of approximately 0.7936 MWh of thermal energy during the charging process, while during reverse flow discharge, there was approximately 0.6538 MWh of thermal energy recovered. The residual thermal energy that was not recovered is approximately 0.1397 MWh which was retained in the basalt material.

Since the residual thermal energy was still present in the storage material, the net energy that was added during each successive charging process was computed by subtracting the residual energy from the total stored energy after each charging process. The residual thermal energy rose at the start but ultimately stabilized at approximately 0.1552 MWh.

The cycle recovery efficiency was computed using the following:

$$\eta_{\text{cycle},n} = \frac{E_{\text{recovered},n}}{E_{\text{added},n}} \times 100,$$

where

$$E_{\text{added},n} = E_{\text{end-charge},n} - E_{\text{start},n}.$$

The cycle recovery efficiency for the first four cycles was approximately 82.39%, 98.01%, 99.81%, and 99.98%, respectively. After approximately Cycles 4-5, the difference between the net thermal energy added during the charging and thermal energy recovered became negligible. At cyclic

steady-state operation, the net thermal energy gained during the charging process as well as the thermal energy recovered became equal to 0.6897 MWh per cycle. As external heat loss and thermal radiation are not taken into account in this model, the thermal energy does not increase any further when the cyclic steady state is achieved. Hence,

$$Q_{\text{in}} \approx Q_{\text{out}}$$

and the recovery efficiency becomes close to 100%.

4.6 Thermal Energy Recovery

The thermal energy recovered during the discharging process was determined by integrating the useful heat transferred to the airflow over the entire discharging period:

$$E_{recovered} = \int \dot{m} C_p (T_{out} - T_{in})\, dt \tag{35}$$

For the first charge–discharge cycle, the numerical model predicted a total recovered thermal energy of

$$E_{recovered} = 0.653814 \text{ MWh} \tag{36}$$

which corresponds to a first-cycle thermal recovery ratio of approximately 82.39% relative to the energy stored at the end of the first charging process.

Table 3 Discharging Performance

Parameter	Value
Discharging duration	8 h
Air inlet temperature	100°C
Initial average basalt temperature	496.78°C
Final average basalt temperature	169.87°C
Final outlet-air temperature	237.23°C
Recovered thermal energy	0.653814 MWh
First-cycle thermal recovery ratio	82.39%

5 Discussion

The numerical results demonstrate the transient nature of the basalt thermal energy storage system during both charging and discharging. The temperature profiles show that the storage medium does not heat uniformly. During charging, the basalt sections located near the hot-air inlet heat first because they are continuously exposed to the highest air temperature. As heat is transferred to the basalt, the air temperature decreases along the tank, causing the downstream sections to heat more slowly. This produces the moving thermal front observed in the charging results.

After eight hours of charging, the average basalt temperature reached approximately 496.78°C rather than the hot-air inlet temperature of 600°C. Consequently, the stored energy was approximately 0.7936 MWh, below the theoretical 1 MWh storage capacity. This difference is expected because the 1 MWh value represents the theoretical energy required to heat the entire basalt mass

uniformly from 100°C to 600°C. Under transient operation, complete thermal equilibrium is not reached within the eight-hour charging period.

The outlet-air temperature reached approximately 407.67°C at the end of charging. This relatively high outlet temperature indicates that part of the thermal energy supplied by the hot air leaves the storage tank without being absorbed by the basalt. The finite convective heat transfer coefficient and the decreasing temperature difference between the air and basalt as charging progresses limit the rate of heat transfer. This behavior explains why extending the charging time or improving the air-to-basalt heat transfer could increase thermal utilization.

The thermal energy stored after eight hours of charging was approximately 0.7936 MWh, corresponding to 79.36% of the theoretical 1 MWh storage capacity. The difference between the theoretical capacity and the actual stored energy is primarily associated with the transient heat-transfer process, since the theoretical capacity assumes uniform heating of the entire basalt mass from 100°C to 600°C, whereas complete thermal equilibrium is not reached during the eight-hour charging period.

During reverse-flow discharging, the average basalt temperature decreased from approximately 496.78°C to 169.87°C after eight hours, while 0.6538 MWh of thermal energy was recovered. This corresponds to approximately 82.39% of the energy stored during the first charging period. The remaining thermal energy is associated with the residual temperature of the basalt at the end of discharge, since the storage medium does not return to its initial temperature of 100°C.

Repeated-cycle study revealed that there was initially an accumulation of residual thermal energy that later led to convergence towards cyclic steady-state performance. As seen after the first discharge, 0.1397 MWh of thermal energy had been stored within the basalt rock. Hence, there is a higher thermal level to be attained in the subsequent charging cycle other than the initial 100°C value. The residual thermal energy increased during the initial cycles and eventually stabilized at approximately 0.1552 MWh.

As the system moved closer to the cyclic steady-state performance, there was a gradual reduction of the difference between the thermal energy charged and discharged. By approximately Cycles 4–5, both values converged to approximately 0.6897 MWh per cycle. The end-of-charge and end-of-discharge average basalt temperatures also converged to 522.42°C and 177.58°C, respectively.

As there are no external thermal losses or thermal radiation losses considered in the current numerical model, there is no further accumulation of thermal energy after achieving cyclic steady-state condition. Hence, the total thermal energy gained during charging is equivalent to the total thermal energy lost during discharging,

Qin Qout,

and hence, the cycle efficiency approaches 100%.

Overall, the results demonstrate that the proposed basalt TES configuration can store and recover a substantial fraction of the available thermal energy over a daily charge–discharge cycle. However, the results also identify heat-transfer-rate limitations and finite charging and discharging durations as important limitations. The current numerical model assumes constant thermophysical properties and neglects heat losses to the surroundings and thermal radiation. Therefore, the calculated performance represents an idealized thermal model, and these effects should be considered in further development of the system.

6 Limitations and Future Work

The current model serves as an initial assessment of the transient thermal behavior of the suggested basalt thermal energy storage system. However, some considerations and assumptions need to be taken into account when interpreting the findings.

First, it was assumed that the thermophysical properties of both the basalt rock and air were constant during the process of charging and discharging. However, this is not the case since the thermophysical properties change with temperature. It is thus recommended that the properties be dependent on temperature.

Secondly, heat losses from the storage tank to the surroundings have been neglected. Therefore, the present model depicts an ideally insulated storage system. In future studies, heat transfer through the wall and insulation of the tank should be considered.

Thermal radiation has also been neglected in the existing model of heat transfer. Given that the charging air temperature can reach 600°C, thermal radiation might be one of the modes of heat transfer. Therefore, future modeling should consider thermal radiation.

This numerical model utilizes a one-dimensional axial model that breaks up the storage tank into 20 control volumes. This model is capable of modeling the motion of the thermal front within the storage tank; however, this model does not capture the radial gradient or variation in the flow around individual basalt rods. A more complex numerical model would allow further study into this phenomenon.

Detailed transient analysis has been carried out with respect to basalt sensible heat storage. While Solar Salt and Magnesium Sulfate Hydrate have been identified as alternatives to TES material, there is no transient model developed for them. Future work can be carried out for these alternative materials and compare their performance with basalt.

Lastly, this study makes use of numerical simulation and does not include any experimental validation of the results. Future work can be carried out by developing a prototype setup in laboratory scale and determining temperature profiles during charge and discharge of thermal energy. Experimental validation of the results can be conducted using these results.

7 Conclusion

In this project, an industrial waste heat recovery and energy storage system is evaluated, and basalt is chosen to analyze the sensible energy storage system. Sensible energy storage system with basalt involves rods with 30 mm in diameter and 3 m in length with the total storage capacity of 1 MWh.

After 8 h charging process, the average temperature of the basalt is 496.78°C, and the stored energy of 0.7936 MWh was found, which corresponds to 79.36% of the theoretical storage capacity. In the first reverse-flow discharge, the recovered energy of 0.6538 MWh was obtained, which leads to the first cycle recovery ratio of 82.39%.

Based on the ten-cycle analysis, cyclic steady-state operation is achieved after four to five cycles. Under cyclic steady-state operation, the residual energy stabilizes at 0.1552 MWh, whereas the net charging and recovered energy converge to 0.6897 MWh/cycle. In the present model, where the external heat loss and thermal radiation are disregarded, $Q_{in} \approx Q_{out}$, therefore, the cycle recovery efficiency approaches 100%.

References

1. T. Nahhas, X. Py, and N. Sadiki, "Experimental Investigation of Basalt Rocks as Storage Material for High-Temperature Concentrated Solar Power Plants," *Renewable and Sustainable Energy Reviews*, vol. 110, pp. 226–235, 2019, doi: 10.1016/j.rser.2019.04.060.
2. M. M. Kenisarin, "High-Temperature Phase Change Materials for Thermal Energy Storage—A Review," *Renewable and Sustainable Energy Reviews*, vol. 14, no. 3, pp. 955–970, 2010.
3. C. J. Ferchaud, R. A. A. Scherpenborg, H. A. Zondag, and R. de Boer, "Thermochemical Seasonal Solar Heat Storage in Salt Hydrates for Residential Applications—Influence of the Water Vapor Pressure on the Desorption Kinetics of $MgSO_4 \cdot 7H_2O$," *Energy Procedia*, vol. 57, pp. 2436–2445, 2014, doi: 10.1016/j.egypro.2014.10.252.
4. F. Marongiu, S. Soprani, and K. Engelbrecht, "Modeling of High Temperature Thermal Energy Storage in Rock Beds—Experimental Comparison and Parametric Study," *Applied Thermal Engineering*, vol. 163, p. 114355, 2019.
5. H. Sadeghifar, N. Djilali, and M. Bahrami, "A Compact Closed-Form Nusselt Formula for Laminar Longitudinal Flow Between Rectangular/Square Arrays of Parallel Cylinders with Unequal Row Temperatures," *International Journal of Thermal Sciences*, vol. 100, pp. 248–254, 2016.
6. D. W. Green and M. Z. Southard, *Perry's Chemical Engineers' Handbook*, 9th ed. New York, NY, USA: McGraw-Hill Education, 2019.
7. Sandia National Laboratories, "Correlation Heat Transfer Coefficient," *Aria User Manual, Version 5.24*, Correlation Heat Transfer Coefficient Reference, Hausen correlation for laminar flow with entrance effects.